Conformational Gating of Long Distance Electron Transfer through Wire-like Bridges in Donor−Bridge−Acceptor Molecules

William B. Davis, Mark A. Ratner, and Michael R. Wasielewski*

Contribution from the Department of Chemistry and Center for Nanofabrication and Molecular Self-Assembly, Northwestern University, Evanston, Illinois 60208-3113

Received February 6, 2001

Abstract: A series of five donor−bridge−acceptor (DBA) molecules in which the donor is tetracene, the acceptor is pyromellitimide, and the bridge molecules are oligo-*p*-phenylenevinylenes (OPV) of increasing length has been shown to undergo electron transfer (ET) by means of two mechanisms. When the bridge is short, strongly distance dependent superexchange dynamics dominates, whereas when the bridge is longer, bridge-assisted hopping dynamics prevails. The latter mechanism results in relatively soft distance dependence for ET in which the OPV oligomers act effectively as molecular wires. We now report studies on the critical influence that bridge dynamics have on electron transfer through these oligomers. The temperature dependence of the charge separation (CS) rates in all five molecules does not appear to obey the predictions of standard ET theories based upon the Condon approximation. All five molecules show behavior consistent with CS being "gated" by torsional motion between the tetracene donor and the first bridge phenyl ring. This is based on the near equivalence of the CS activation energies measured for all five molecules with the frequency of a known vibrational mode in 5-phenyltetracene. In the molecule containing a *trans*-stilbene bridge, a competition occurs between the tetracene−phenyl torsional motion and one that occurs between the vinyl group and the phenyls linked to it. This results in complex temperature-dependent CS that exhibits both activated and negatively activated regimes. The charge recombination (CR) reactions within the molecules which have the two shortest bridges, namely phenyl and *trans*-stilbene, show a weaker dependence on these molecular motions. The three molecules with the longest bridges all display complex temperature dependencies in both their rates of CS and CR, most likely because of the complex torsional motions, which arise from the multiple phenyl−vinyl linkages. The data show that long-distance electron transfer and therefore wire-like behavior within conjugated bridge molecules depend critically on these low-frequency torsional motions. Molecular device designs that utilize such bridges will need to address these issues.

Introduction

Progress toward a fundamental understanding of electron transfer (ET) reactions has come from an intricate tapestry of theoretical tools and techniques, new methods in synthetic chemistry, and the development of spectroscopic apparatus capable of spanning the time range from femtoseconds to hours. Early theoretical treatments of electron transfer come from the work of Marcus[1,2] and Hush,[3,4] which itself is an extension of transition state theory. Later theories, such as those developed by Jortner[5] and Fischer and Van Duyne[6] (henceforth referred to as semiclassical ET theory), incorporate the quantum mechanical nature of high-frequency solvent and intramolecular vibrational modes that are coupled to the ET reaction coordinate. From the work of several groups,[5−8] the rate of thermal, nonadiabatic ET between a donor and acceptor assuming a single high-frequency vibration can be written as

$$k_{ET} = \frac{2\pi}{\hbar}|H_{DA}|^2\sqrt{\frac{1}{4\pi\lambda k_B T}}\sum_{n=0}^{\infty}\exp[-S]\frac{S^n}{n!}\exp\left[\frac{-(\Delta G^\circ + \lambda + n\hbar\omega)^2}{4\lambda k_B T}\right] \quad (1)$$

In eq 1, k_B is the Boltzmann constant, T is temperature, ΔG° is the free energy change of the electron-transfer reaction, ω is the frequency of the coupled quantum mechanical vibrational mode, and λ is the reorganization energy for all classical modes. In general, λ will contain contributions from both solvent polarization, λ_s, and low-frequency intramolecular vibrations, λ_{Low}. S is the Huang−Rhys factor, mathematically expressed as $S = \lambda_i/\hbar\omega$, where λ_i is the reorganization energy for the quantum mechanical vibrational mode.

When both electron tunneling and vibrational motion occur on the same time scale, a breakdown of the Condon approximation can occur, which implies that H_{DA} within eq 1 becomes dependent upon the nuclear coordinates. Under these circumstances, the electronic motion can be completely controlled, or "gated",[9−11] by the nuclear motions within the electron donor−

(1) Marcus, R. A. *J. Chem. Phys.* **1956**, *24*, 966−978.
(2) Marcus, R. A. *Annu. Rev. Phys. Chem.* **1964**, *15*, 155−196.
(3) Hush, N. S. *J. Chem. Phys.* **1958**, *28*, 962−972.
(4) Hush, N. S. *Trans. Faraday Soc.* **1961**, *57*, 577−580.
(5) Jortner, J. *J. Chem. Phys.* **1976**, *64*, 4860−4867.
(6) Fischer, S. F.; van Duyne, R. P. *Chem. Phys.* **1977**, *26*, 9−16.
(7) DeVault, D. *Quantum Mechanical Tunneling in Biological Systems*; Cambridge University Press: Cambridge, 1984.
(8) Hopfield, J. J. *Proc. Natl. Acad. Sci. U.S.A.* **1974**, *71*, 3640−3644.
(9) Hoffman, B. M.; Ratner, M. A. *J. Am. Chem. Soc.* **1987**, *109*, 6237−6243.

10.1021/ja010330z CCC: $20.00
Published on Web 07/19/2001

acceptor molecule. Expressions describing the temperature and free energy dependencies of k_{ET} must be reevaluated under these circumstances.[12] Equation 1, which is derived for the high-temperature limit, nevertheless predicts an Arrhenius-like temperature dependence for k_{ET}. In particular, when reactions occur at high temperature in the Marcus normal region, where the driving force is smaller than the total reorganization energy, Marcus theory is often adequate.[13−15] However, for reactions occurring in the Marcus inverted region, the influence of high-frequency vibrational modes[5,6,16,17] can lead to ET rate constants with very weak temperature dependence, or even complete temperature independence.[7,15,18−20] Non-Arrhenius temperature dependence can also be found in ET systems in which slow solvent relaxation controls the ET reaction.[21−29] This is especially pronounced in glass forming organic solvents and proteins, where the temperature dependence of the ET rate constants will change below the glass transition temperature of the medium.[30−36]

Of all the vibrational modes available to conjugated organic donor−bridge−acceptor (DBA) molecules, those associated with donor−bridge and bridge−acceptor torsional motions are expected to contribute the most to variation of H_{DA}. In addition, any other torsional motions within D, B, or A will also contribute. From the McConnell analysis of electronic coupling in organic radical exchange reactions,[37] H_{DA} can be approximated in the following form[38−44]

$$H_{DA} = \frac{V_{DB}V_{BA}}{\omega_{DB}}\left(\frac{V_{BB}}{\omega_{DB}}\right)^{N-1} \quad (2)$$

In eq 2, V_{DB} and V_{BA} are the electronic coupling strengths of the donor and bridge and bridge and acceptor, respectively, V_{BB} is the electronic coupling between bridge sites, ω_{DB} is the energy gap between the relevant states of the donor and bridge, and N is the number of identical bridge sites. Equation 2 is approximate and does not take into account nonnearest neighbor interactions and multiple pathways.[42] Torsional motions will primarily affect the electronic coupling between adjacent electronic sites, and will impart an angular dependence to V_{ij} (i,j nearest neighbors) of the form

$$V_{ij} = V_{ij}^{0}\cos(\Phi) \quad (3)$$

where Φ is the torsional angle and V_{ij}^{0} is the electronic coupling between sites i and j at $\Phi = 0°$. If Φ is temperature dependent, this will impart a temperature dependence to H_{DA} that may override the normal Arrhenius-like temperature dependence of k_{ET} expected from semiclassical ET theory. For example, the Condon approximation will fail when conformations with small Boltzmann populations have anomalously large H_{DA} values.

The above discussion of the temperature dependence of H_{DA} assumes that the ET system under consideration falls into a superexchange regime. In particular, for eq 2 to hold, the requirements of second-order perturbation theory must be met by a particular DBA molecule. Several theoretical treatments have now been developed to describe DBA systems in which ET does not occur via the superexchange mechanism.[45−50] In particular, the most important situation in which the superexchange mechanism breaks down occurs when the energy gap between donor and bridge (or acceptor and bridge) is of the same order of magnitude as the electronic coupling between the donor and the bridge, V_{DB}. When the energy gap separating electron donor and bridge becomes small, the rate-limiting step of the ET reaction becomes thermal promotion of the electron from the donor to the bridge. This promotion occurs primarily through the coupled vibrational modes, and the observed activation energy is approximately the energy gap separating donor and bridge. The implication of this result is that the bridge becomes a real intermediate state with electronic population residing on it for finite times. This contrasts with superexchange, where the bridge serves as a tunneling barrier separating the donor and acceptor, and electronic population does not usually reside on it for any reasonable time. In this paper, we describe the temperature dependence of both photoinduced charge separation (CS) and thermal charge recombination (CR) in the DBA series, **1**−**5**,[51] which undergoes a change in electron-transfer mechanism from superexchange to bridge localization

(10) Bechtold, R.; Kuehn, C.; Lepre, C.; Isied, S. S. *Nature* **1986**, *322*, 286−288.
(11) Brunschwig, B. S.; Sutin, N. *J. Am. Chem. Soc.* **1989**, *111*, 7454−7465.
(12) Beratan, D. N.; Hopfield, J. J. *J. Chem. Phys.* **1984**, *81*, 5753−5759.
(13) Kroon, J.; Oevering, H.; Verhoeven, J. W.; Warman, J. M.; Oliver, A. M.; Paddon-Row: M. N. *J. Phys. Chem.* **1993**, *97*, 5065−5069.
(14) O'Driscoll, E.; Simon, J. D.; Peters, K. S. *J. Am. Chem. Soc.* **1990**, *112*.
(15) Liang, N.; Miller, J. R.; Closs, G. L. *J. Am. Chem. Soc.* **1989**, *111*, 8740−8741.
(16) Bixon, M.; Jortner, J. *J. Phys. Chem.* **1991**, *95*, 1941−1944.
(17) Kestner, N. R. *J. Phys. Chem.* **1980**, *84*, 1270−1275.
(18) Rehm, D.; Weller, A. *Isr. J. Chem.* **1970**, *8*, 259−271.
(19) Gunner, M. R.; Dutton, P. L. *J. Phys. Chem.* **1989**, *93*, 3400−3412.
(20) Smit, K. J.; Warman, J. M.; de Haas, M. P.; Paddon-Row, M. N. *Chem. Phys. Lett.* **1988**, *152*, 177−182.
(21) Zusman, L. D. *Chem. Phys.* **1980**, *49*, 295−304.
(22) McGuire, M.; McLendon, G. *J. Phys. Chem.* **1986**, *90*, 2549−2551.
(23) Sumi, H.; Marcus, R. A. *J. Chem. Phys.* **1986**, *84*.
(24) Rips, I.; Jortner, J. *Chem. Phys. Lett.* **1987**, *133*, 411−414.
(25) Akesson, E.; Johnson, A. E.; Levinger, N. E.; Walker, G. C.; de Bruil, T. P.; Barbara, P. F. *J. Chem. Phys.* **1992**, *96*, 7859−7862.
(26) Grote, R. F.; Hynes, J. T. *J. Chem. Phys.* **1981**, *74*, 4465−4475.
(27) Heitele, H.; Michel-Beyerle, M. E.; Finckh, P. *Chem. Phys. Lett.* **1987**, *138*, 237−243.
(28) Rempel, U.; von Maltzan, B.; von Borczyskowski, C. *Z. Phys. Chem.* **1991**, *170*, 107−116.
(29) Wiederrecht, G. P.; Svec, W. A.; Wasielewski, M. R. *J. Phys. Chem. B* **1999**, *103*, 1386−1389.
(30) Harrison, R. J.; Pearce, B.; Beddard, G. S.; Cowan, J. A.; Sanders, K. M. *Chem. Phys.* **1987**, *116*, 429−448.
(31) Chen, P.; Danielson, E.; Meyer, T. J. *J. Phys. Chem.* **1988**, *92*, 3708−3711.
(32) Gaines, G. L.; O'Neill, M. P.; Svec, W. A.; Niemczyk, M. P.; Wasielewski, M. R. *J. Am. Chem. Soc.* **1991**, *113*, 719−721.
(33) Harriman, A.; Heitz, V.; Ebersole, M.; van Willigen, H. *J. Phys. Chem.* **1994**, *98*, 4982−4989.
(34) Hoffman, B. M.; Natan, M. J.; Nocek, J. M.; Wallin, S. A. *Struct. Bonding* **1991**, *75*, 85−108.
(35) Hoffman, B. M.; Ratner, M. A. *Inorg. Chim. Acta* **1996**, *243*, 233−278.
(36) Agmon, N.; Rabinovich, S. *J. Chem. Phys.* **1992**, *97*, 7270−7286.
(37) McConnell, H. M. *J. Chem. Phys.* **1961**, *35*, 508−515.
(38) Ratner, M. A. *J. Phys. Chem.* **1990**, *94*, 4877−4883.
(39) Evenson, J. W.; Karplus, M. *Science* **1993**, *262*, 1247−1249.
(40) Meade, T. J. *Metal Ions in Biological Systems*; Sigel, A., Sigel, H., Eds.; Marcel Dekker: New York, 1996; Vol. 33, p 453.
(41) Miller, J. R.; Beitz, J. V. *J. Chem. Phys.* **1981**, *74*, 6746−6756.
(42) Beratan, D. N.; Betts, J.; Onuchic, J. N. *Science* **1991**, *252*, 1285−1288.
(43) Hsu, C. P.; Marcus, R. A. *J. Chem. Phys.* **1997**, *106*, 584−598.
(44) Onipko, A. *Chem. Phys. Lett.* **1998**, *292*, 267−272.
(45) Skourtis, S.; Mukamel, S. *Chem. Phys.* **1995**, *197*, 367−388.
(46) Davis, W. B.; Wasielewski, M. R.; Ratner, M. A.; Mujica, V.; Nitzan, A. *J. Phys. Chem. A* **1997**, *101*, 6158−6164.
(47) Segal, D.; Nitzan, A.; Davis, W. B.; Wasielewski, M. R.; Ratner, M. A. *J. Phys. Chem. B* **2000**, *104*, 3817−3829.
(48) Okada, A.; Chernyak, V.; Mukamel, S. *J. Phys. Chem. A* **1998**, *102*, 1241−1251.
(49) Felts, A. K.; Pollard, W. T.; Friesner, R. A. *J. Phys. Chem.* **1995**, *99*, 2929−2940.
(50) Pollard, W. T.; Felts, A. K.; Friesner, R. A. *Adv. Chem. Phys.* **1996**, *93*, 77−134.
(51) Davis, W. B.; Svec, W. A.; Ratner, M. A.; Wasielewski, M. R. *Nature* **1998**, *396*, 60−63.

Chart 1

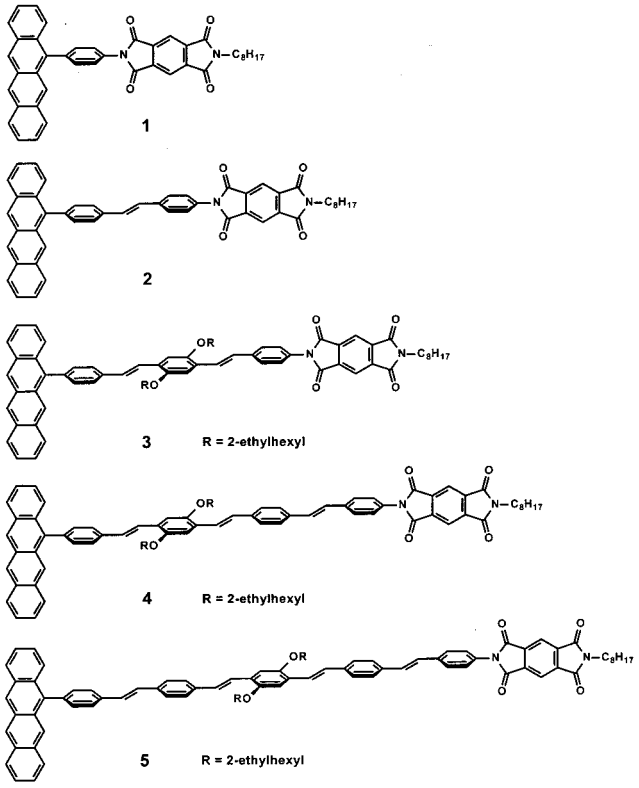

dynamics as the distance between the donor and acceptor is increased. This results in a wire-like, soft distance dependence of the electron-transfer rates. This series of molecules employs a tetracene (TET) electron donor, a pyromellitimide (PI) electron acceptor, and oligo-*p*-phenylenevinylene (OPV) bridges. At room temperature, when the two shortest bridges, benzene and *trans*-stilbene, are used, the electron-transfer rates show a steep distance dependence in 2-methyltetrahydrofuran (MTHF). However, when OPV oligomers containing either three, four, or five phenyl rings are used as the bridges, the rates of charge separation are *faster* than those measured through the two shorter bridges (benzene or *trans*-stilbene) and the charge separation rates show a very weak distance dependence. In the studies reported here, the temperature dependence of the charge separation (k_{CS}) and charge recombination (k_{CR}) rates of **1**−**5** in the glass forming solvent MTHF were studied from room temperature down to 77 K, which is well below the 110 K glass transition temperature of MTHF. In addition, these rate constants for **3** were measured down to 8 K. The motivation of this work is to compare and contrast the temperature dependence of the ET rates in the two different regimes, superexchange vs bridge hopping. We find that the temperature dependence of k_{CS} can be assigned to a breakdown of the Condon approximation in all five molecules. In particular, we find evidence for gating of the donor to acceptor electron transfer by specific vibrational modes, which control H_{DA} via torsional motion of the donor relative to the bridge, as well as torsional motion between adjacent bridge sites. These molecular motions can have a profound effect on the ability of conjugated molecules to transport charge for long distances.

Results

Transient absorption spectra of **1** following selective excitation of TET with a 150 fs, 483 nm pump pulse at 298 (10.5 ps) and 170 K (40 ps) are shown in Figure 1. The intense band at

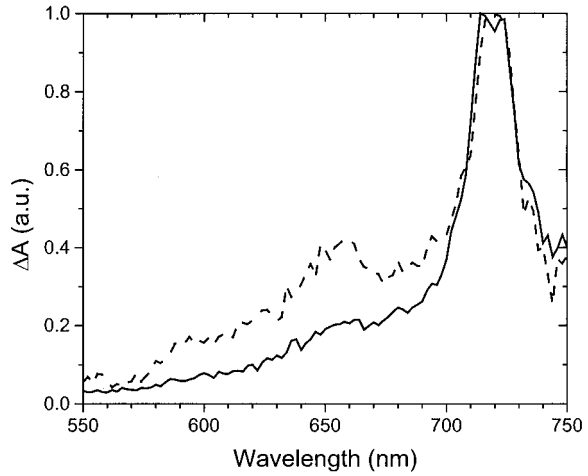

Figure 1. Transient absorption spectra of **1** in MTHF, obtained at 298 (—) and 170 K (- - -). These spectra were taken 10.5 and 40 ps, respectively, after the arrival of a 150 fs, 483 nm pump pulse at the sample. The data were normalized to a value of 1.0 at 720 nm in both plots to accentuate the differences between the two spectra.

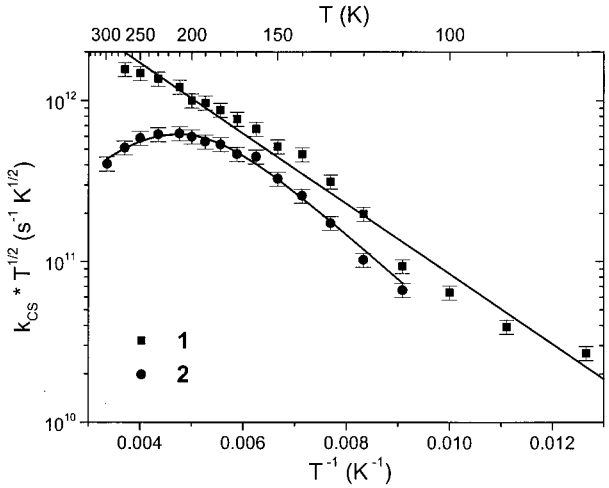

Figure 2. Plots of log k_{CS} $T^{1/2}$ vs T^{-1} for **1** and **2** in MTHF.

720 nm is due to the formation of PI^{-}.[52] These spectra show that lowering the temperature results in relatively minor changes. The most notable change is a sharpening of the first vibronic band of PI^{-} at 660 nm. The raw rate constants for CS and CR within **1**−**5** in MTHF at all the temperatures measured are listed in the Supporting Information. Given the functional form of eq 1, the CS rate constants are assumed to be of the form $k_{CS} = A' T^{-1/2} \exp(-E_a/k_B T)$. The temperature dependence data for **1** and **2** are plotted as $\log(k_{CS}T^{1/2})$ vs T^{-1} for CS in Figure 2. The CS rate constants for **1** were fit to a straight line using linear least-squares regression to yield $E_a = 349 \pm 12$ cm^{-1} and $A' = 1.28(\pm 0.16) \times 10^{13}$ s^{-1} K$^{1/2}$ with an acceptable quality of fit ($R = 0.991$). In contrast, fitting a plot of log k_{CS} vs T^{-1} to a straight line (not shown) yields an R value of only 0.952, indicating that the Arrhenius prefactor most likely has a $T^{-1/2}$ temperature dependence associated with it as predicted by eq 1.

While the CS rate constants for **1** strictly increase with increasing temperature, the CS rate constants for **2** show a turnover from activated behavior at low temperatures to a negatively activated regime above $T = 210$ K, Figure 2. To see

(52) Gosztola, D.; Niemczyk, M. P.; Svec, W. A.; Lukas, A. S.; Wasielewski, M. R. *J. Phys Chem. A* **2000**, *104*, 6545−6551.

Table 1. Arrhenius Prefactor and Activation Energy for the CS Rates of **1**−**5** in MTHF

molecule	temp range	E_a (cm^{-1})	A' (s^{-1})	R
1	120 K ≤ T ≤ 230 K	349 ± 12	1.28(±0.16) × 10^{13}	0.991
2	110 K ≤ T ≤ 210 K	366 ± 27	9.69(±2.48) × 10^{12}	0.986
3	120 K ≤ T ≤ 230 K	353 ± 11	4.20(±0.39) × 10^{13}	0.996
4	120 K ≤ T ≤ 210 K	373 ± 18	3.33(±0.50) × 10^{13}	0.991
5	120 K ≤ T ≤ 298 K	349 ± 13	1.99(±0.21) × 10^{13}	0.993

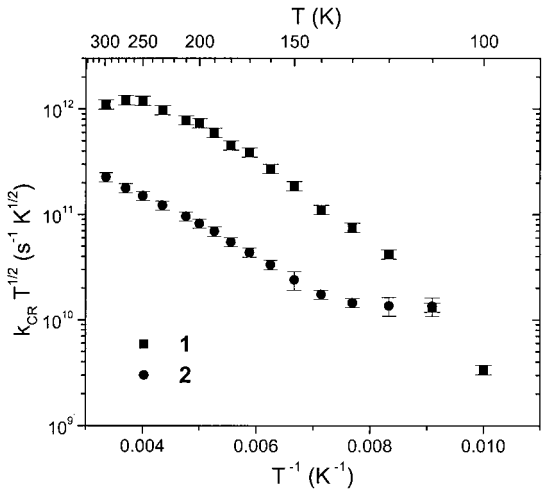

Figure 3. Plots of log k_{CR} $T^{1/2}$ vs T^{-1} for **1** and **2** in MTHF.

if the temperature dependence for the CS rate constants in **2** in the low-temperature activated region between 110 and 210 K can be described by semiclassical ET theory, these data were plotted as log($k_{CS}T^{1/2}$) vs T^{-1}, and the data fit to a straight line (not shown). The *R*-value of this fit, $R = 0.977$, was not as good as that for a linear fit to the CS data for **1**. The values of the parameters E_a and A' from the fit to the CS data of **2** have the values 366(±27) cm^{-1} and 9.69(±2.48) × 10^{12} s^{-1} K$^{1/2}$, respectively. Thus the measured values of E_a and A' from the fits to the CS data are very similar for **1** and **2**, and are summarized in Table 1. In addition, Figure 2 shows that the magnitudes of the CS rate constants for **1** and **2** differ by only about a factor of 2 over the temperature range 210 K ≥ T ≥ 110 K. The line drawn through the temperature dependence data for **2** shown in Figure 2 is a nonlinear least-squares fit to a kinetic model that will be described below.

A comparison of the temperature dependencies of the corresponding CR rate constants for **1** and **2** is shown in Figure 3. The data for **1** and **2** are distinct from one another, both in magnitude and in thermal behavior. For **1**, the CR rates are essentially temperature independent at high temperatures, then decrease with decreasing temperature below $T \sim 230$ K. In contrast, the CR rates measured for **2** appear to be thermally activated from room temperature down to ~140 K, after which they show little if any temperature dependence. The results of a linear least-squares fit of the function $k_{CR} = A' T^{-1/2} \exp(-$

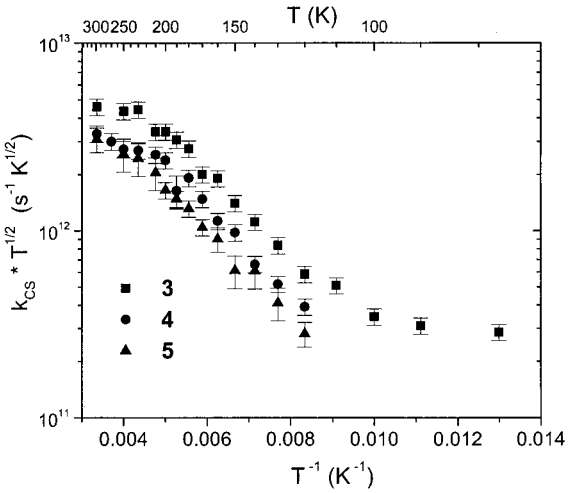

Figure 4. Plots of log k_{CS} $T^{1/2}$ vs T^{-1} for **3**, **4**, and **5** in MTHF.

E_{CR}/k_BT) to the CR data for **1** and **2** over the temperature ranges within which the data display linear activated behavior are presented in Table 2. The values of E_a are somewhat larger for CR than those exhibited by the CS reactions. A comparison of the CS and CR rate constants in **1** (Figures 1 and 2) shows that at high temperatures the electron transfer occurs with nearly the same rate in both the forward and reverse directions, but at low temperatures (T < 190 K) the rate of CR slows down with respect to the CS rate. In molecule **2**, the CR rate constants are always less than those of CS and the two sets of data do not appear to be correlated in any way.

The temperature dependencies of the CS and CR rate constants in **3**−**5** were also measured in MTHF. The data for **3** extend from room temperature down to 8 K. The data for **4** and **5** only extend from room temperature to 120 K because these molecules are photochemically labile in the MTHF glass. Figure 4 shows a plot of the CS data obtained from molecules **3**−**5**. All three molecules show similar behavior above the T_g of MTHF (~110 K), namely a region of temperature independence at high temperatures, followed by a region of thermal activation at lower temperatures. At $T \leq 120$ K the CS rates for **3** become temperature independent.

The three sets of CS data in Figure 4 were fit to the equation $k_{CS} = A' T^{-1/2} \exp(-E_a/k_BT)$, over the temperature range in which linear behavior was observed using a linear least-squares fitting routine to obtain E_a and A', Table 1. As the bridge gets longer, A' decreases and E_a appears to stay the same. Even more striking is the similarity between these activation energies and those measured for **1** and **2** in the same temperature region. The activation energies measured using data obtained between 120 and 210 K are the same for all five DBA molecules within experimental error.

The temperature dependencies of the CR rate constants in **3**−**5** are also very similar to one another, Figure 5. Molecules **3** and **4** exhibit monoexponential CR kinetics near room

Table 2. Arrhenius Prefactor and Activation Energy for the CR Rates of **1**−**5** in MTHF

molecule	component	temp range	E_a (cm^{-1})	A' (s^{-1})	R
1		120 K ≤ T ≤ 250 K	549 ± 19	3.45(±0.52) × 10^{13}	0.994
2		140 K ≤ T ≤ 298 K	460 ± 8	2.15(±0.13) × 10^{12}	0.998
3	slow	100 K ≤ T ≤ 230 K	331 ± 11	1.12(±0.11) × 10^{11}	0.994
	fast	79 K ≤ T ≤ 200 K	291 ± 17	3.79(±0.70) × 10^{11}	0.986
4	slow	120 K ≤ T ≤ 210 K	446 ± 19	1.30 (±0.21) × 10^{11}	0.993
	fast	120 K ≤ T ≤ 190 K	507 ± 28	2.12 (±0.52) × 10^{12}	0.994
5	slow	160 K ≤ T ≤ 250 K	210 ± 24	3.59 (±0.60) × 10^{10}	0.962
	fast	120 K ≤ T ≤ 170 K	505 ± 26	4.86 (±1.11) × 10^{12}	0.995

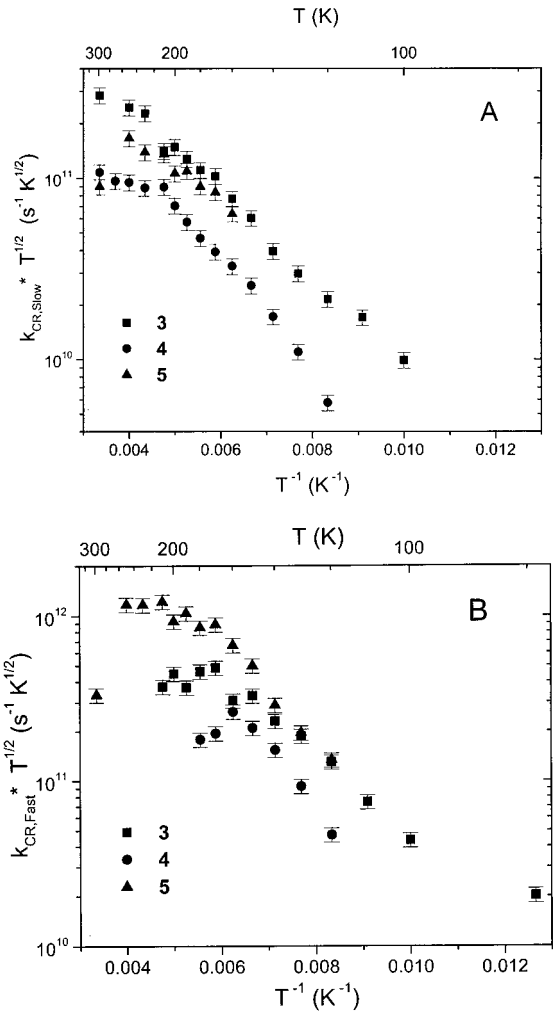

Figure 5. Plots of log $k_{CR}\ T^{1/2}$ vs T^{-1} for **3**, **4**, and **5** in MTHF: (A) slow kinetic component and (B) fast kinetic component.

temperature, which become biexponential at lower temperatures. The turnover from mono- to biexponential CR kinetics occurs at 210 K in **3** and at 190 K in **4**. As the temperature decreases, the fast/slow amplitude ratio of the two components increases, and at low temperatures, the faster component is completely dominant. In **5**, biexponential kinetics are already seen at room temperature, and the fast/slow amplitude ratio increases with decreasing temperature, similar to what is observed for **3** and **4**. Figure 5 shows the dependencies of the fast and slow CR rate constants of **3**−**5** on temperature. For **3** and **4**, the amplitudes of the slow CR components, Figure 5A, display a region of temperature independence at high temperatures, as well as a region of activated behavior at temperatures below 200 K. The slow CR rates in **5** increase as the temperature decreases from room temperature to 250 K, after which these rates strictly decrease with decreasing temperature. The amplitudes of the fast CR components for **3** and **4** in Figure 5B are thermally activated over their entire temperature range. The fast CR rates in **5** increase as the temperature is lowered from room temperature to 250 K, show a region of temperature independence from 250 to 170 K, then decrease with decreasing temperature.

The fast and slow CR rates in **3**−**5** were all fit to the equation $k_{CR} = A'\ T^{-1/2}\ \exp(-E_a/k_BT)$ in the temperature regions where they show thermally activated behavior. The results of these least-squares fits are listed in Table 2, along with the temperature regions over which activated behavior is seen in the fast and slow CR rates of **3**−**5**. The fit of this functional form to the CR data of **3**−**5** is good in general, except for the fast rates in **3** and the slow rates in **5**. For each of the three compounds, the fast and slow CR rates do not have Arrhenius prefactors or activation energies that match within the uncertainty of the fits. Therefore, it appears as if the fast and slow CR rates arise from two different processes occurring in all three molecules.

Discussion

The CS and CR reactions within molecules **1**−**5** exhibit complex temperature dependencies. As one might expect, the degree of complexity increases as the number of torsional motions within these DBA molecules increases. These data will be analyzed in a stepwise fashion beginning with the molecules having the two shortest bridges. A precise description would require analyzing the motion of the photogenerated wave packet on the full multidimensional geometric space of the molecule. A reasonable picture, more in the tradition of chemical state language, will prove more helpful, and we adopt this approach in describing the decay dynamics associated with the CS and CR processes.

Molecules 1 and 2. Apart from the explicit temperature dependence of k_{ET} expressed in eq 1, ΔG and λ are also temperature dependent. The standard assumption for aromatic organic π donors and acceptors is that an ET reaction will couple to a high-frequency vibrational mode of about 1500 cm^{-1}, the frequency of a C=C stretch, and that λ_i has a value close to 0.3 eV.[53] The electronic coupling matrix element H_{DA} is usually assumed to be temperature independent (the Condon approximation).

Weller derived the following equation for the free energy of an ion-pair state, based upon the dielectric continuum model of solvation:[54]

$$\Delta G_{IP}{}^{0} = E_{OX} - E_{RED} - \frac{e^2}{\epsilon_s R_{DA}} + e^2\left(\frac{1}{2R_D} + \frac{1}{2R_A}\right)\left(\frac{1}{\epsilon_s} - \frac{1}{\epsilon_s'}\right) \tag{4}$$

where E_{OX} and E_{RED} were defined above, e is the electronic charge, ϵ_s is the static dielectric constant of the solvent in which the rate constants are measured, ϵ_s' is the dielectric constant of the solvent in which E_{OX} and E_{RED} are measured, R_{DA} is the donor-to-acceptor center-to-center distance, and R_D and R_A are the spherical radii of the donor and acceptor, respectively. The free energies for the CS and CR reactions are calculated using

$$\Delta G_{CS}{}^{\circ} = -E_{0-0} + \Delta G_{IP}{}^{\circ}$$
$$\Delta G_{CR}{}^{\circ} = -\Delta G_{IP}{}^{\circ} \tag{5}$$

where E_{0-0} is the energy of the lowest excited singlet state of the photoexcited donor. These equations assume that the zero of the energy scale corresponds to the energy of the ground-state molecule. Equation 5 indicates that the temperature dependence of both ΔG_{CS} and ΔG_{CR} arises from the corresponding dependence of ΔG_{IP}. In turn, the temperature dependence of ΔG_{IP} is principally a function of the temperature dependence of ϵ_s because the redox potentials within the Weller treatment are determined in a polar solvent with dielectric constant ϵ_s' at room temperature. While the utility of the Weller treatment has been questioned for solvents of low polarity, the

(53) Closs, G. L.; Calcaterra, L. T.; Green, N. J.; Penfield, K. W.; Miller, J. R. *J. Phys. Chem.* **1986**, *90*, 3673−3683.
(54) Weller, A. *Z. Phys. Chem.* **1982**, *133*, 93−98.

Table 3. $\Delta G_{CS}°$ and λ_s at 298 K Calculated for Molecules **1**−**5** Using Eqs 4−6

molecule	R_{DA} (Å)	$-\Delta G_{CS}°$ (eV)	λ_s (eV)
1	11.1	0.81	0.83
2	17.7	0.74	1.0
3	24.3	0.71	1.1
4	30.9	0.69	1.1
5	38.0	0.67	1.2

use of eq 4 to estimate ΔG_{IP} in solvents of moderate polarity yields reasonable results.[55]

Again drawing upon dielectric continuum theory,[1,2] Marcus showed that λ_s can be approximated from the following equation:

$$\lambda_s = e^2\left(\frac{1}{2R_D} + \frac{1}{2R_A} - \frac{1}{R_{DA}}\right)\left(\frac{1}{\epsilon_\infty} - \frac{1}{\epsilon_s}\right) \qquad (6)$$

where ϵ_∞ is the optical dielectric constant of the solvent and the remaining parameters are defined above. The temperature dependence of λ_s is due to that of ϵ_∞ and ϵ_s. The utility of using continuum models for predicting the temperature dependence of λ_s in highly dipolar media has been questioned recently.[56] These deviations may be diminished somewhat in solvents of more modest polarity like MTHF. As an approximation eqs 4−6 are used to calculate $\Delta G_{CS}°$ and λ_s for molecules **1**−**5** at 298 K, which are listed in Table 3. The values of $R_D = 4.9$ Å and $R_A = 3.4$ Å, as well as the values of R_{DA} listed in Table 3, were obtained from MM+ optimized geometries.[57] For MTHF, $\epsilon_\infty = 1.97$ and $\epsilon_s = 6.97$ at 298 K.[58] The one-electron oxidation and reduction potentials, E_{OX} and E_{RED}, for TET and PI are 0.77 and −0.79 V vs SCE, respectively, in butyronitrile ($\epsilon_s' = 24.8$[58]). The experimental temperature dependence of ϵ_s for MTHF at $T \geq 140$ K is accurately described by the equation $\epsilon_s(T) = 3.1 + 860/(T - 73)$, while at lower temperatures, after MTHF has entered into a glassy state, $\epsilon_s = 2.6$.[59] The temperature dependence of ϵ_∞ is assumed to vary linearly from 1.97 at 298 K to 15.2 at 77 K (see Supporting Information). The values of ϵ_∞ around and below the T_g of MTHF are suspect because of the large changes in solvent properties that occur at the glass transition. However, they will be used here with the caveat that any data that are calculated at those temperatures are considered highly approximate.

Equation 1, along with eqs 4−6 can be used to estimate the value of H_{DA} for **1** and **2** using the measured values of k_{ET} at 298 K along with the other parameters listed above. Doing so gives H_{DA} values of 50 and 48 cm^{-1} for **1** and **2**, respectively. Assuming that H_{DA} is temperature independent, as well as using the temperature-dependent values of $\Delta G_{CS}°$ and λ_s, eq 1 predicts the CS rate constant temperature dependencies for **1** and **2** shown in Figure 6. The predicted CS rate constants for both **1** and **2** are only weakly temperature dependent, and do not reproduce the experimentally determined temperature dependencies.

Since the rate constants for CS within **1** and **2** are large and the CS process is weakly activated for $T \leq 210$ K, it is possible that the observed temperature dependence results from a breakdown of the Condon approximation. There are two common structural features present in both **1** and **2**. The first is the attachment of a phenyl group to the tetracene donor, and the second is the attachment of a phenyl group to the pyromellitimide acceptor. Since there are other donor−bridge−acceptor molecules that incorporate a phenyl bound to pyromellitimide and obey semiclassical ET theory,[60,61] a molecular motion associated with this linkage is probably not responsible for Condon breakdown. It is therefore useful to focus on the tetracene−phenyl linkage.

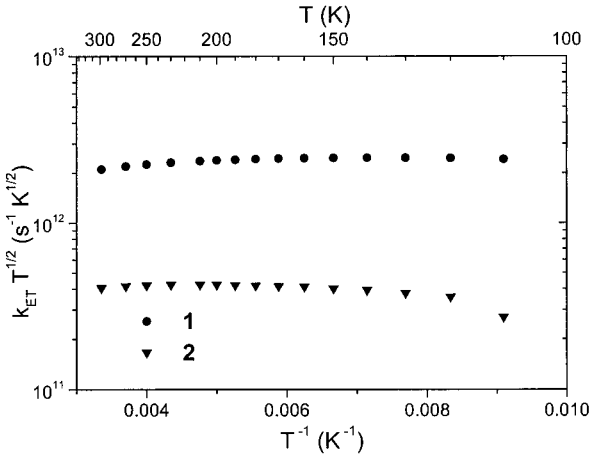

Figure 6. Plots of log $k_{CS} T^{1/2}$ vs T^{-1} for **1** and **2** in MTHF using rate constants predicted by eq 1 using temperature-dependent values of ΔG_{CS} and λ.

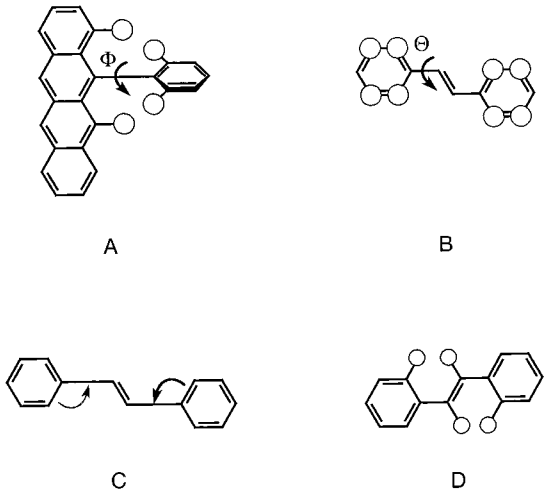

Figure 7. Tetracene−bridge and intrabridge torsions and vibrations within **1**−**5**.

In the ground state of 5-phenyltetracene (**Ph-TET**), the dihedral angle, Φ, between the tetracene π system and the phenyl π system is reasonably large, ∼69° according to MM+ calculations. This accounts for the reasonably weak electronic coupling between tetracene and the phenyl group seen in the absorption spectra of 5-(*p*-tolyl)tetracene.[51] In the S_1 state of **Ph-TET**, $\Phi \sim 60°$,[62] which is a rather modest change in dihedral angle from the ground state. Since $\pi-\pi$ electronic coupling depends on cos Φ, the electronic coupling between the tetracene chromophore and the phenyl ring is expected to

(55) Oevering, H.; Paddon-Row, M. N.; Heppener, M.; Oliver, A. M.; Cotsaris, E.; Verhoeven, J. W.; Hush, N. S. *J. Am. Chem. Soc.* **1987**, *109*, 3258−3269.

(56) Vath, P.; Zimmt, M. B.; Matyushov, D. V.; Voth, G. A. *J. Phys. Chem. B* **1999**, *103*, 9130−9140.

(57) Optimized geometries of **1**−**5** were obtained using the MM+ force field within Hyperchem 5.01a (Hypercube, Waterloo, Ont.).

(58) *CRC Handbook of Chemistry and Physics*, 70th ed.; CRC Press: Boca Raton, FL, 1989.

(59) Furutsuka, T.; Imura, T.; Kojima, T.; Kawabe, K. *Osaka Univ. Eng. Rep.* **1974**, *24*, 367.

(60) Osuka, A.; Nagata, T.; Naruyama, K.; Mataga, N.; Asahi, T.; Yamazaki, I.; Nishimura, Y. *Chem. Phys. Lett* **1991**, *185*, 88−94.

(61) Wiederrecht, G. P.; Svec, W. A.; Wasielewski, M. R. *J. Phys. Chem. B* **1999**, *103*, 1386-1389.

be similar in the S_0 and S_1 states of tetracene. There is a torsional barrier in the S_1 state of **Ph-TET** that impedes the tetracene and phenyl group from reorienting into a more coplanar geometry. The physical origin of this barrier is steric hindrance between the hydrogens at the 4 and 6 positions of tetracene and the hydrogens at the ortho positions of the phenyl ring, Figure 7A. The attachment of a phenyl group to the 5-position of tetracene results in a significant enhancement of a 296 cm^{-1} out-of-plane vibration of tetracene.[62] This vibrational mode is thought to lower the torsional barrier in the S_1 state of **Ph-TET** by displacing the tetracene hydrogen atoms enough to allow the phenyl group to rotate into a more coplanar configuration. Thus, the following reaction scheme is proposed for **1**:

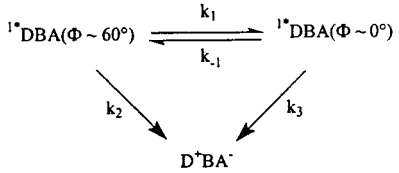

(7)

Since the donor and acceptor are in an unfavorable geometry for CS when Φ is 60°, we can assume that $k_1 \gg k_2$. Also, we assume that $k_3 \gg k_1$, k_{-1} because of strong donor−bridge electronic overlap in a planar geometry. Under these conditions, the observed CS rate in **1** will be k_1, which is the rate of torsional motion between the tetracene donor and phenyl bridge. This kinetic scheme and accompanying assumptions about the magnitudes of the rate constants contained within are able to explain why the dominant thermal contribution to the temperature dependence of k_{CS} in **1** appears to be due to the tetracene−phenyl torsional rearrangement. The kinetic schemes used to analyze the results depend on equilibria between a small number of conformations. While distributions of conformations undoubtedly exist, our data do not exhibit distributed kinetics. This is most likely a consequence of narrow conformational distributions.

Lowering the torsional barrier between the tetracene donor and the phenyl or stilbenyl bridge allows more efficient electronic coupling between the donor and acceptor in **1** and **2**. The torsional barrier is high at low temperatures because the 296 cm^{-1} vibrational mode is inactivated, resulting in relatively weak electronic coupling between the donor and acceptor, and hence a slower CS rate. Raising the temperature activates the out-of-plane vibrational mode, lowering the torsional barrier and allowing the donor and bridge to assume a more favorable geometry for charge transport. It is intriguing that the frequency of this mode, 296 cm^{-1} in the gas phase, is very similar to the activation energy measured for the CS rates of **1** at all temperatures measured, and the activation energy of k_{CS} of **2** at $T \leq 210$ K.

While the thermal activation of this tetracene vibrational mode might explain the low-temperature data for **1** and **2**, it cannot account for the high-temperature turnover in k_{CS} seen experimentally for **2**. Again, the chemical structures of **1** and **2** can be examined for clues as to what is causing the differences in the CS dynamics of these two donor−acceptor molecules. Both molecules have the tetracene−phenyl and phenyl−pyromellitimide linkages, but only **2** has an intervening vinyl group between the donor and acceptor. In the ground state, *trans*-stilbene has a very anharmonic torsional mode about its vinyl group, which causes distortions from planarity.[63−66] The flexibility of this torsional mode, coupled with its low zero point frequency, ~8 cm^{-1}, leads to strong coupling of this mode to other vibrational modes in *trans*-stilbene. The normal mode displacements of this stilbene torsional mode are shown in Figure 7B. Even in the lowest vibrational level, the potential of this torsional mode is predicted to have turning points at ±22°, indicating there are large deviations from planarity in *trans*-stilbene even at low temperatures.[63] Since electronic coupling through a *trans*-stilbene bridge will approximately scale like cos Θ, where Θ is the dihedral angle between the phenyl and vinyl groups, decreasing the temperature will result in an *increase* in the electronic coupling. Therefore, this torsional motion is expected to exhibit a negative activation energy, which is in fact found for the high-temperature CS rates in **2**.

Assuming that the tetracene−bridge and stilbene torsional modes lead to a break down of the Condon approximation, the following kinetic scheme is proposed to explain the experimental CS rates in molecule **2**.

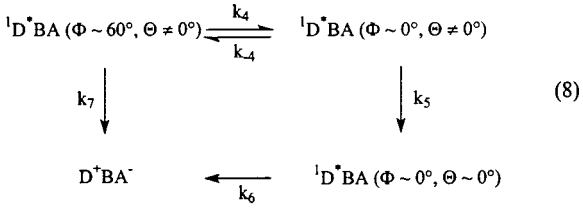

(8)

The rate constants k_4 and k_{-4} describe the forward and backward isomerization rates for the tetracene−phenyl torsional mode, k_5 is the isomerization rate of the stilbene torsional mode, and k_6 is the rate at which the electron moves from donor to acceptor, once the molecule has assumed the optimum geometry for ET (assumed to be $\Phi \sim 0°$, $\Theta \sim 0°$). The rate of the donor-to-acceptor ET reaction in the initial excited-state geometry, k_7, is assumed to be negligible as compared to k_4 because of weak electronic coupling between the donor and acceptor in the ($\Phi \sim 60°$, $\Theta \neq 0°$) geometry. Using the steady-state approximation, the rate of formation of ^{1}D*BA ($\Phi \sim 0°$, $\Theta \sim 0°$), k_{planar}, is given by

$$k_{planar} = \frac{k_5 k_4}{k_5 + k_{-4}} = \frac{k_5 k_4}{k_5 + (k_4/K_4)} \qquad (9)$$

where K_4 is the equilibrium constant between the two tetracene−phenyl conformers. If $k_{planar} \gg k_6$, the rate of formation of the ion-pair state will be dominated by k_6 and the observed ET dynamics should follow the temperature behavior predicted by semiclassical ET theory. However, if $k_{planar} \leq k_6$, k_{planar} will be observed experimentally. Since the temperature dependence of the CS rates in **2** does not appear to follow standard theories of ET, it is assumed that the inequality $k_{planar} \leq k_6$ holds. Therefore the torsional dynamics of **2** control the observed CS rates, $k_{obs} = k_{planar}$. Because k_4 has a positive activation energy and k_5 has a negative activation energy, at high temperatures $k_4 \gg k_5$ and $k_{obs} \sim K_4 k_5$. At low temperatures, the opposite limit should be seen: $k_5 \gg k_4$ and $k_{obs} \sim k_4$. Therefore, at high temperatures k_{obs} should be an increasing function with decreas-

(62) Löhmannsröben, H.-G.; Bahatt, D.; Even, U. *J. Phys. Chem.* **1990**, *94*, 4025−4029.

(63) Suzuki, T.; Mikami, N.; Ito, M. *J. Phys. Chem.* **1986**, *90*, 6431−6440.

(64) Syage, J. A.; Felker, P. M.; Zewail, A. H. *J. Chem. Phys.* **1984**, *81*, 4685−4705.

(65) Haller, K.; Chiang, W.-Y.; del Rosario, A.; Laane, J. *J. Mol. Struct.* **1996**, *379*, 19−23.

(66) Spangler, L. H.; van Zee, R.; Zwier, T. S. *J. Phys. Chem.* **1987**, *91*, 2781−2786.

ing temperature due to the behavior of k_5. As the temperature decreases further, the rates should turn over and k_{obs} decrease with decreasing temperature because of k_4. Assuming $k_4 = A'_4T^{-1/2}\exp(-E_{a4}/k_BT)$ and $k_5 = A'_5T^{-1/2}\exp(-E_{a5}/k_BT)$, eq 9 can be used to fit the experimental data, Figure 2. For simplicity, K_4 was given a value of 1, and the best fit to the experimental data gave the following values for the other four model parameters: $A'_4 = 2.57(\pm 2.04) \times 10^{13}$ s^{-1} K$^{1/2}$, $E_{a4} = 447 \pm 94$ cm^{-1}, $A'_5 = 5.53(\pm 1.45) \times 10^{10}$ s^{-1} K$^{1/2}$, and $E_{a5} = -460 \pm 58$ cm^{-1}. Varying K_4 did not lead to an appreciable improvement in χ^2 for the fit, so only the data obtained with $K_4 = 1$ will be discussed. The values of E_{a4} and A'_4 are similar to the Arrhenius parameters obtained previously from the CS rates of **2** from 210 K $\geq T \geq$ 110 K, as well as those obtained for **1**. The activation energy of k_5 is indeed negative.

The assignment of the negative activation energy to a single coupled, higher frequency, vibrational mode in *trans*-stilbene is complicated by the extreme anharmonicity of the torsional mode. For instance, in the ground-state vibrational spectrum of *trans*-stilbene there are a large number of overtone and combination bands, which should not have significant population normally. Out of all the low-frequency vibrational modes in *trans*-stilbene, there is one that shows a large coupling to the torsional motion of the phenyl-vinyl linkage with a frequency of 413 cm^{-1}. The assignment of this vibrational mode is still somewhat ambiguous,[63,64] but it has been tentatively assigned to an in-plane bending motion of the phenyl rings about the vinyl group. The qualitative behavior of this A_g symmetric mode is shown in Figure 7C.[65] This vibrational mode may couple strongly to the torsional mode of stilbene because as the phenyl rings move toward the vinyl group, there should be steric repulsion between the ortho hydrogens on the phenyl rings and the vinylic hydrogens, Figure 7D. Thermal activation of this symmetric mode might push the phenyl rings out of plane to minimize repulsion between the hydrogens.

Since the CS rates are controlled primarily by intramolecular torsions, the CR rates may be sensitive to these molecular motions as well. Since CS in **1** occurs at an optimized, nonequilibrium geometry near the top of the tetracene−phenyl torsional barrier, there must be kinetic competition between CR back down to the ground state and geometrical relaxation of the donor and bridge to a twisted geometry in the ion-pair state. A kinetic scheme that describes these dynamics is outlined as follows:

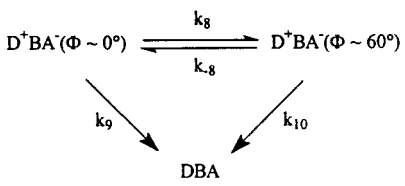

(10)

In eq 10, it is assumed that the relaxed geometry between the donor and bridge in the ion-pair state is located at $\Phi \sim 60°$. Rate constant k_9 is should be larger than k_{10} at all temperatures because the electronic coupling between D^+ and B in the planar ion-pair state is larger than that in the twisted ion-pair state. Thus, at all temperatures the observed rate constant for CR will depend principally on competition between k_8 and k_9. If $k_9 \gg k_8$, the observed CR rate constant will be k_9, which should have a weak temperature dependence due to the strong electronic coupling between nearly coplanar D^+ and B. On the other hand, if $k_8 \gg k_9$ and $k_8 \gg k_{-8}$, the observed CR rate constant is k_{10}. The weak temperature dependence for CR observed at high temperatures suggests that $k_9 \gg k_8$ in that regime. As the temperature decreases, eq 1 predicts that k_9 should decrease. At the same time, k_8 should increase due to the negatively activated nature of this process. Thus, at low temperatures the observed CR rate constant is k_{10}. The kinetic scheme in eq 10 describes the experimental CR rates if $k_8 \gg k_{10} \gg k_{-8}$ at all temperatures and $k_9 \gg k_8$ at high temperatures. Thus, it appears that torsional motion between the twisted and planar donor−bridge states does not kinetically control the CR dynamics of **1**. However, on a cautious note, the equilibrium constant of the donor−bridge torsional motion could change once CS has occurred and CR commences depending on how strongly the torsional mode will couple with other vibrational modes once tetracene becomes a radical cation. Unfortunately, no experimental data concerning this torsional−vibrational coupling in the 5-phenyltetracene radical cation, or any other related systems, are available.

Just as in molecule **1**, there may be competition between CR and torsional relaxation in **2**. The data in Figure 3 show that for 298 K > T > 150 K, the CR reaction exhibits a single positive activation energy, $E_{aCR} = 450$ cm^{-1}. On the basis of the fact that E_{aCR} is positive, the negatively activated phenyl−vinyl torsional motion, which must be very rapid throughout this temperature range, has little or no influence on the CR rates. Thus, the same arguments developed for CR in **1** using eq 10 can be applied to CR in **2**. As a result, invoking the donor−bridge torsional motion is not necessary to explain the temperature dependence of CR for 298 K > T > 150 K.

At temperatures below the T_g of MTHF, the CR rates become temperature independent. This behavior has been seen before in protein ET complexes. Perhaps the most famous example is that of the cytochrome−photosynthetic reaction center complex from the organism *Chromatium vinosum*.[67,68] In this protein complex, the rate constant for ET from the cytochrome to the oxidized reaction center is nearly temperature independent below 100 K, while above 100 K it is thermally activated. This behavior can be described by semiclassical ET theory, which assigns the temperature dependence seen at high temperatures to an activated barrier crossing, while the ET rates are dominated by nuclear tunneling at low temperatures.[5,6] The similarity between the qualitative behavior seen in the CR rates of **2** with the predictions of semiclassical ET theory indicates that the CR dynamics in **2** probably follow the Condon approximation at all the temperatures studied.

Molecules 3−5. In the previous section it was argued that changes in the tetracene−phenyl torsional angle are responsible for the temperature dependence of k_{CS} in **1** and **2**. This same torsional motion could control the CS rates of **3**−**5** at temperatures above the T_g of MTHF as well. In our earlier work on **1**−**5** at 298 K we observed a superexchange ET mechanism in **1** and **2** and a hopping ET mechanism in **3**−**5**.[51] It is useful to examine whether the kinetic scheme proposed earlier to account for the CS data in **3**−**5** at 298 K can also be used to describe the temperature dependence data presented here:[51]

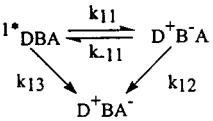

(11)

(67) DeVault, D.; Chance, B. *Biophys. J.* **1966**, *6*, 825.
(68) DeVault, D.; Parkes, J. H.; Chance, B. *Nature* **1967**, *215*, 642−644.

The steady-state solution to this equation gives the following prediction for the observed ET rate constant, k_{obs}

$$k_{obs} = k_{13} + \frac{k_{12}k_{11}}{k_{12} + k_{-11}} \cong \frac{k_{12}k_{11}}{k_{12} + k_{-11}} \qquad (12)$$

The last equality in eq 12 is assumed to hold for molecules **3**−**5**, where the direct donor-to-acceptor charge-transfer rate, k_{13}, is assumed to be small based on the trend established by the CS rates of **1** and **2**. When $k_{12} \gg k_{-11}$ in eq 12, $k_{obs} \sim k_{11}$, and when $k_{12} \ll k_{-11}$, $k_{obs} \sim K_{11}k_{12}$, where K_{11} is the equilibrium constant for reaction 11. Since k_{12} describes the charge shift reaction between the bridge and acceptor, it may have a weak temperature dependence since charge transfer from the bridge to the acceptor is strongly exergonic. The rate constants k_{11} and k_{-11} describe the rates of promotion of an electron from the donor onto the bridge and vice versa. These two rate constants should be strongly influenced by torsional motion between the tetracene donor and first phenyl attached to it. At high temperatures this motion should be rapid, and both k_{11} and k_{-11} may be larger than k_{12}. Therefore, the observed rate of charge transport will be dominated by k_{12}, which is expected to possess a weak temperature dependence. This may explain the observed weak temperature dependence of the CS rate constants of **3**−**5** at high temperatures. As the temperature decreases, k_{11} and k_{-11} decrease, $k_{12} \gg k_{11}$ and k_{-11}, and the observed CS rate should be dominated by k_{11}. Thus, the kinetics of the donor−bridge torsional motion should be the rate-limiting step at lower temperatures, consistent with the similarity of the activation energy of CS in all five ET molecules at temperatures between 200 and 120 K.

It is uncertain if the rates of CS in **4** and **5** become temperature independent at low temperatures. At temperatures at or below T_g for MTHF, slowing solvent dynamics will strongly affect the observed rate constants. However, for **3** data were obtained at lower temperatures and the rates do indeed become temperature independent. Just as in *trans*-stilbene, the OPV oligomers are expected to have anharmonic torsional potentials associated with each of the vinyl linkages. Analyzing this multiple rotor problem in detail is beyond the scope of this paper. However, some qualitative arguments about their behavior can be made. As the temperature decreases, the geometry of the OPV bridge should become more planar overall because the large-amplitude torsional motions about the vinyl linkages diminish. Once MTHF enters into a glassy state, these motions should be nearly absent in the molecule. As the bridge becomes more planar, the energy of its LUMO is expected to decrease. Because the bridge LUMO and the donor LUMO are nearly degenerate at room temperature in **3**−**5**,[52] enhanced conjugation in the bridge at low temperatures could serve to bring the donor and bridge LUMOs into resonance. This would cause the temperature dependence of the CS rates in **3**−**5** to become activationless at low temperatures, as is observed experimentally in **3**.

Turning now to the CR rates in **3**−**5**, the most notable feature of the data is the observed biexponential kinetics. In our previous work on these molecules,[51] it was argued that the following kinetic scheme described the CR dynamics at room temperature:

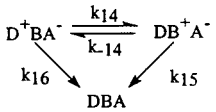

(13)

Molecules **3**−**5** display hole-hopping dynamics during the CR reaction, as well as electron hopping during the CS reaction. In the CS reaction, the energy gap between the ^{1}D*BA and D$^+$B$^-$A states dictates whether the superexchange and hopping electron transport mechanisms dominate. Likewise, the energy gap between the D$^+$BA$^-$ and DB$^+$A$^-$ states controls the hole hopping CR dynamics. The energy gap between these two ion-pair states is expected to change dramatically with temperature in **3**−**5** because of structural changes in the OPV bridges. All three bridges are expected to have the same out-of-plane phenyl−vinyl torsional motion as the stilbene bridge in **2**; however, now there are multiple vinyl groups in each bridge. As the number of rotors increases in these bridges, their potential surfaces should become increasingly complex with multiple barriers and extrema. In fact, numerous torsional conformations of the bridge coexist at high temperatures, and the experimental CR data reflect the ensemble average. As the temperature decreases, the bridges are expected to become more planar similar to the behavior of *trans*-stilbene.

The nonplanar conformations of the OPV bridges at room temperature should keep the ion-pair energy gap relatively large, and turn off hole hopping dynamics. In **3** and **4**, this results in monoexponential CR decays at high temperatures because $k_{16} \gg k_{14}$ in eq 13. As the temperature decreases, the OPV bridges should become more planar, and hence the energy gap between D$^+$BA$^-$ and DB$^+$A$^-$ should decrease. Due to the complex torsional landscape in these bridges, some molecules should be in a more planar geometry, while others may get trapped in twisted local minima, thus **3** and **4** exhibit biexponential kinetics. As the temperature is decreased further, k_{14} is expected to increase because of the decreasing donor−bridge energy gap, while k_{15} remains fast at all temperatures because of strong electronic coupling between B$^+$ and A$^-$. Thus, k_{14} will dominate the observed CR rates in **3** and **4** at low temperatures and the observed CR decays will return to monoexponential kinetics.

While the CR rate constants for **3** and **4** display the same qualitative behavior in Figure 5, the rate constants for **5** differ. Even at room temperature the fast decay component dominates the CR dynamics. The fast rates in **5** increase dramatically as the temperature is lowered from 298 to 250 K, and then level out before decreasing as the temperature decreases further. Over the temperature range 298 K $\geq T \geq$ 200 K, the fast CR rate constants in **5** are larger than all the CR rate constants in **3** and **4**. This behavior most likely arises from the D$^+$BA$^-$ and DB$^+$A$^-$ states becoming resonant in **5** near room temperature. From eq 4, at 298 K the energy of the D$^+$BA$^-$ ion-pair state is 1.88 eV, while that of the corresponding DB$^+$A$^-$ ion-pair state is 1.91 eV. The energy difference between these two ion-pair states at 298 K is only 0.03 eV, or 242 cm^{-1}. A similar analysis yields D$^+$BA$^-$ − DB$^+$A$^-$ energy gaps of 0.16 eV (1300 cm^{-1}) in **3** and 0.08 eV (650 cm^{-1}) in **4**. A small change in the planarity of the OPV bridge in **5**, induced by a small decrease in the temperature, is probably sufficient to bring the two ion-pair states D$^+$BA$^-$ and DB$^+$A$^-$ into resonance. This would account for the strong biexponential kinetics for CR seen at room temperature in **5**. Because the ion-pair state energy gaps are larger in **3** and **4**, biexponential CR kinetics are not observed in these compounds until the temperature is decreased. Resonance between the D$^+$BA$^-$ and DB$^+$A$^-$ states in **5** would also account for the fast and slow CR rates not behaving like those seen in **3** and **4**.

Conclusions

Long conjugated molecules appear at first glance to be ideally suited for incorporation into donor−bridge−acceptor assemblies

designed to carry out long distance charge transport. However, an important aspect of these long π bridges that is often neglected is their propensity for significant conformational flexibility due to low-frequency vibrational modes. The results presented here show that low-frequency vibrations of the tetracene donor and the OPV oligomers exert significant control over the ET rates in **1**−**5**, which results in conformational gating of the ET reaction. In addition, these results serve as a warning about neglecting bridge dynamics when analyzing both the distance and temperature dependence of ET reactions. Other conjugated bridges,[69−71] such as poly(phenylene), poly(thiophene), and poly(phenylene-ethynylene), are also strong candidate systems for investigating the role of conformational gating in photoinduced ET reactions. In addition, many of these concepts can be explored further by preparing molecules in which complex gating motions are restricted by the structure of the donor−bridge−acceptor molecule.

Experimental Section

Compounds **1**−**5** were synthesized using methods described in the Supporting Information. The structures of these compounds were confirmed using ^{1}H NMR and mass spectral data.

Cyclic voltammetry (CV) and bulk electrolysis were carried out using a potentiostat and voltage ramp programmer (Princeton Applied Research, Models 173 and 175) and a standard three-electrode arrangement. CV measurements used platinum working and auxiliary electrodes as well as a saturated sodium calomel reference electrode (SSCE). All electrochemical measurements were carried out in N_2-purged butyronitrile with 0.1 M Bu_4NClO_4 as the supporting electrolyte. The scan rate for CV measurements was typically 50−100 mV/s. Ferrocene was used as an internal redox standard for all measurements.

Ground state optical absorption measurements were recorded using a computer controlled spectrophotometer (Shimadzu, Model 1601). Femtosecond transient absorption measurements were obtained with 150 fs, 483 nm pump pulses and a 130 fs white light continuum probe pulse produced by an amplified-Ti:sapphire laser system with an optical parametric amplifier (OPA) as described previously.[72] The total instrument function is 180 fs. The concentrations of **1**−**5** used for transient absorption measurements were approximately 100 μM in 2 mm path length cells. Both pump beams and the probe beam were 200 mm in diameter with the 483 nm pump beam having an energy of 0.5 μJ at the sample.

For variable temperature experiments down to 77 K, a liquid nitrogen cooled optical dewar (Janis Research VPS-100) was utilized, while for experiments down to 8 K a liquid helium optical dewar (Janis Research STVP-100) was utilized. The MTHF solvent used for each experiment was freshly distilled and subjected to 3 freeze−pump−thaw cycles immediately before use. All samples were prepared under a nitrogen atmosphere to minimize the presence of oxygen. Each spectroscopic sample was placed in a sealed, homemade, 2 mm path length optical cell constructed from two transparent quartz windows and a 2 mm wide Teflon spacer. After seating the sample holder in the dewar, the dewar was evacuated to $\sim 10^{-3}$ Torr of pressure. The sample temperature was maintained to within $\pm$0.5 K by a Lake Shore Cryotronics Model DRC-82C temperature controller. The sample temperature was lowered from room temperature down to the solvent glass transition temperature ($\sim$110−120 K for MTHF) by 10 to 20 deg increments. The sample was allowed to equilibrate for 15−20 min at each new temperature before data collection. After reaching the glass transition temperature, the sample temperature was cooled all the way down to the temperature of liquid nitrogen ($\sim$77 K), or liquid helium (4.2 K), and warmed back up to the glass transition temperature of the solvent in 10 deg increments. Again, the sample was allowed to equilibrate at each new temperature for a minimum of 15 min before data collection.

Acknowledgment. This work was supported by the Division of Chemical Sciences, Office of Basic Energy Sciences, U.S. Department of Energy under grant no. DE-FG02-99ER14999 (M.R.W.) and by the NSF (M.A.R.). W.B.D. wishes to thank the Link Foundation for a fellowship. The authors wish to thank Mr. Walter A. Svec of Argonne National Laboratory for his assistance in preparing **1**−**5**.

Supporting Information Available: Synthetic and spectroscopic details, as well as temperature dependence of ϵ_∞ (PDF). This material is available free of charge via the Internet at http://pubs.acs.org.

JA010330Z

(69) Helms, A.; Heiler, D.; McLendon, G. *J. Am. Chem. Soc.* **1992**, *114*, 6227−6238.

(70) Osuka, A.; Maruyama, K.; Mataga, N.; Asahi, T.; Yamazaki, I.; Tamai, N. *J. Am. Chem. Soc.* **1990**, *112*, 4958−4959.

(71) Finckh, P.; Heitele, H.; Michel-Beyerle, M. E. *J. Phys. Chem.* **1988**, *92*, 6584−6590.

(72) Lukas, A. S.; Miller, S. E.; Wasielewski, M. R. *J. Phys. Chem. B* **2000**, *104*, 931−940.